# On the Optimal Thermal Management of Hybrid-Electric Vehicles with Heat Recovery Systems.

F. Merz, A. Sciarretta, J.-C. Dabadie, L. Serrano

*Oil & Gas Science and Technology – Rev. IFP Energies nouvelles,* Vol. 67 (2012), No. 4, pp. 601-612

DOI: 10.2516/ogst/2012017

Dossier

*Electronic Intelligence in Vehicles*
Intelligence électronique dans les véhicules

# On the Optimal Thermal Management of Hybrid-Electric Vehicles with Heat Recovery Systems

F. Merz[1], A. Sciarretta[2*], J.-C. Dabadie[2] and L. Serrao[2]

*1 ETH Zurich, Dept. of Mechanical and Process Engineering, Sonnegstr. 3, 8092 Zürich, Switzerland; now with the International Postgraduate Trainee, ZF Friedrichshafen AG, 88038 Friedrichshafen - Germany*
*2 IFP Energies nouvelles, 1-4 avenue de Bois-Préau, 92852 Rueil-Malmaison Cedex - France*
*e-mail: felix.merz2@zf.com (present address) - antonio.sciarretta@ifpen.fr - jean-charles.dabadie@ifpen.fr - lorenzo.serrao@dana.com (present address)*
[*] Corresponding author

**Résumé — Sur le thermo-management optimal d'un véhicule électrique hybride avec un système de récupération de chaleur** — Une approche généralisée pour combiner la gestion de l'énergie (supervision du groupe motopropulseur) et le thermo-management dans les véhicules hybrides électriques est proposée. Un système hybride incluant le post-traitement des polluants et un système de récupération de la chaleur à l'échappement du moteur thermique est simulé pour plusieurs scénarii, y compris le cas de départ à froid. Des stratégies de gestion de l'énergie optimales sont dérivées à partir du Principe de Minimum de Pontriaguine (PMP). Inspirée par les facteurs d'équivalence pour la consommation électrique que l'on retrouve dans la stratégie ECMS, la notion d'équivalent en carburant des flux d'énergie thermique est introduite. Les stratégies dérivées du PMP sont comparées avec une stratégie heuristique basée sur des règles. Les bénéfices en termes d'économies de carburant et réduction des émissions polluantes que l'on trouve pour différents scénarii sont encourageantes.

***Abstract — On the Optimal Thermal Management of Hybrid-Electric Vehicles with Heat Recovery Systems*** *— A general framework to combine optimal energy management (powertrain supervisory control) and thermal management in Hybrid Electric Vehicles (HEV) is presented. A HEV system with engine exhaust aftertreatment and exhaust heat recovery system is simulated under various scenarios, including warm and cold start. Optimal strategies are derived from Pontryagin Minimum Principle (PMP). The concept of fuel equivalent of thermal energy variations – similar to the equivalence factors for battery energy of standard Equivalent Consumption Minimization Strategy (ECMS) – is introduced. The PMP-based strategies are compared with a heuristic, rule-based strategy. The benefits in fuel economy and reduction of pollutant emissions that are obtained for several scenarios are very promising.*

## INTRODUCTION

The contribution of hybrid-electric powertrain technology to future mobility is expected to grow. On one hand, such propulsion systems can improve the rather poor thermal efficiency of standard internal-combustion engines. On the other hand, they pave the way to a partial electrification of individual mobility by combining short-range purely electric travel with long range driving capability (plug-in and extended-range concepts). One distinguishing feature of HEVs is the need for a nontrivial energy management strategy in order to control the energy flow within the vehicle. This supervisory control task has attracted a considerable amount of research in the last fifteen years

(surveys [1-3]). Common energy management strategies are based on heuristic considerations inspired by the expected behavior of the propulsion system. Moreover, optimized strategies have been introduced that are based on the definition of a cost function to be minimized and optimal control to achieve it. The offline version of this paradigm is widely used in the automotive industry to assess the performance of various solutions and to pre-calibrate the online energy management strategies [4-8]. State-of-the-art methods for offline optimization of energy management strategies are dynamic programming and the direct application of Pontryagin's minimum principle (PMP). The optimization problem is usually formulated as follows:

- the cost function is either fuel consumption or engine-out emissions, or a combination of both [9-11], although in [12] the battery ageing has been considered as well;
- the only system dynamics considered are those of the battery State of Charge (SOC);
- the global constraint to the state variable reflects charge-sustaining (final SOC equals initial SOC) or charge-depleting (final SOC is nearly zero [13]) operation.

Recent works have been aimed at extending the standard optimization problem to consider additional scenarios, including multiple electric sources [14, 15], drivability constraints [16, 17] and additional dynamics. Indeed the HEV system has other dynamics than SOC that may be relevant for overall optimization. The most important is obviously the vehicle longitudinal dynamics and thus vehicle speed. However, its optimization is usually out of the scope of energy management and rather concerns look-ahead drive control (or predictive cruise control) [18, 19]. Next in relevance (and the object of this paper) are temperature levels, since thermal phenomena have longer characteristic times than mechanical or electrical phenomena. Temperature is a key factor in many phenomena:

- engine warm-up: fuel consumption and engine-out emissions depend on temperature levels (oil, coolant, block);
- engine cool-down: in HEVs the engine can be turned off and as a result its temperature decreases;
- activation (light-off) of the catalytic converter: effective conversion requires a certain threshold temperature; catalyst temperature dynamics are correlated with those of the engine;
- heat supplies to cabin heater or other uses (demist, defrost);
- heat accumulation systems (tanks, phase-change materials);
- heat recovery systems (Rankine-cycles, thermoelectricity).

Figure 1 shows a schematic of a HEV including its main thermal dynamics, including the engine (coolant, oil and block) temperature $\theta_e$, a heat accumulation system ($\theta_{acc}$), a cold accumulation system ($\theta_{a/c}$) engine exhaust and catalyst system ($\theta_c$) and a heat recovery system ($\theta_r$). Power flows connecting these "thermal reservoirs" are equally depicted.

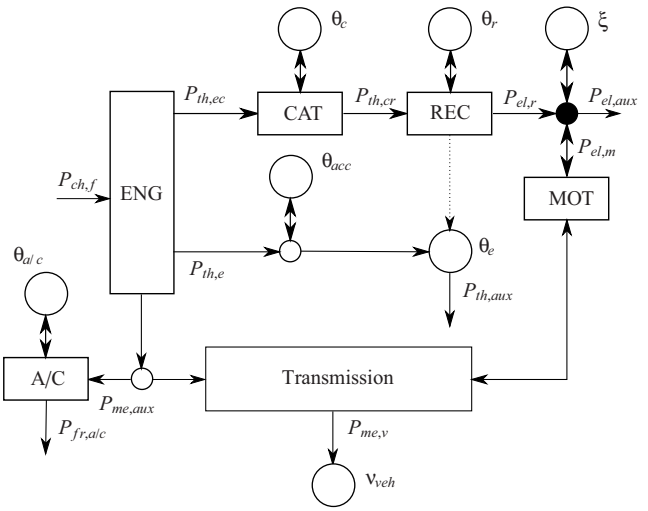


Figure 1

Schematics of a HEV depicting relevant dynamics as "reservoirs" (circles), as well as power flows (arrows) and power converters (blocks).

Besides the early contribution [20], a few recent HEV studies considered at least one thermal dynamic in the optimization strategy. The study [22] represents a first attempt to include the dynamics of $\theta_e$ in a PMP-based optimization and to quantify the fuel corresponding economy benefit. On the other hand [23], describes the implementation of an optimal online strategy, sensitive to $\theta_c$, on a test bench and its advantages over simple heuristics. In [21], stochastic dynamic programming is applied to a plant model that considers $\theta_c$ as a state variable. The same dynamics are considered in [24] but later they are neglected in the controller. The main focus is on minimizing a combination of fuel cost and cost of urea injected in a SCR system, with a limit on tailpipe $NO_x$ emission.

In this paper, a more comprehensive framework for PMP-based offline optimization with inclusion of thermal dynamics is presented. Section 1 presents control-oriented modeling of three dynamics:

- engine thermal dynamics;
- exhaust and catalyst thermal dynamics;
- Rankine-cycle dynamics.

Section 2 presents four optimization scenarios S0–S3, one heuristic strategy RB and four optimal strategies, namely, PMP0–PMP3, which include up to two thermal dynamics. In Section 3, the various strategies are compared for scenarios S0–S3 and simulation results are presented.

## 1 MODELING

### 1.1 Full-Order Model (FOM)

The system considered here is a combined (power-split) hybrid vehicle (1 360 kg curb weight) equipped with a 70 kW gasoline engine, two motors/generators (50 kW and 30 kW) and a 6.9 Ah Li-ion battery. A detailed model of the system was developed and implemented in AMESim [25] (1). The detailed model, labelled here as FOM (Full-Order Model), simulates the mechanical, electrical and thermal phenomena in the HEV, including driver response, combustion mode, temperature corrections for fuel consumption and engine-out emissions, engine torque response, engine control loop dynamics, inertia of electric machines, thermal capacity of engine oil, engine coolant circuit, external cooling circuit with radiator and heat exchangers, exhaust system including three-way catalytic converter, cabin heater and electric auxiliaries. The submodels of various components are linked with each other based on their mechanical, electrical, thermal couplings and on the basis of a physical ("forward") causality.

Due to its comprehensive nature and complexity, the FOM is impractical for control and optimization purposes. Instead, a reduced-order counterpart (ROM) has been derived. Generally speaking, the main thermal dynamics are approximated by lumped temperature levels, while all of the other dynamics are neglected and the corresponding static relationships are used. The choice of the thermal levels to consider depends on the particular optimization scenario under study. Three cases are described in the following subsections.

### 1.2 Engine Temperature

The effect of engine temperature on the fuel consumption rate $m_f$ is modeled in the ROM as:

$$m_f(u, \theta_e) = m_f^\circ(u) \cdot f_{cons}(u, \theta_e) \qquad (1)$$

where $u$ is the engine operating point (see below), $f_{cons}(\cdot)$ is an extra-consumption factor that takes into account the increase of friction and the increase of fuel injected per cycle at low temperatures. Data for warm-engine fuel consumption $m_f^\circ$ are derived from engine tests and implemented in the same way as in the FOM. Data for $f_{cons}$ are derived from:

- extra injection rate tabulated as a function of coolant temperature;
- engine FMEP tabulated as a function of speed and oil temperature, see Figure 2a.

Engine-out emission rates also depend on $\theta_e$ in the ROM, according to the relationship:

$$m_{j,e}(u, \theta_e) = m_j^\circ(u) \cdot \left(1 + (f_j - 1)\frac{\theta_e - \theta_{e,cold}}{\theta_{e,warm} - \theta_{e,cold}}\right) \qquad (2)$$

(1) This work has been carried out in the EU-funded project HICEPS, see http://www.hi-ceps.eu/tutto.htm

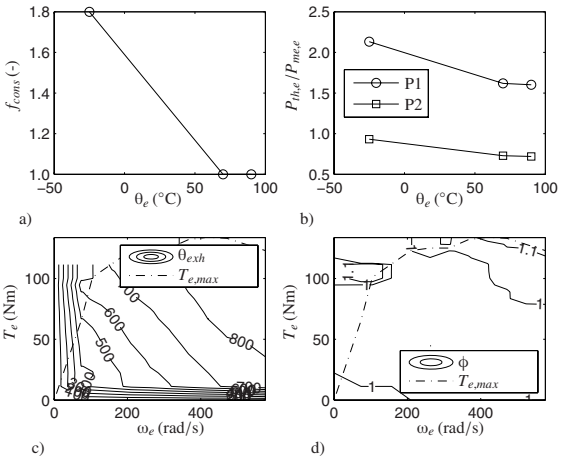


Figure 2

Tabulated data of the engine, a) injection-related cold consumption factor, b) thermal power losses at two operating points (P1: middle-load operating point, P2: high-load operating point), c) exhaust temperature, d) equivalence ratio.

where $j = \{\mathrm{CO}, \mathrm{HC}, \mathrm{NO}_x\}$, $f_j$'s are cold emission factors, $\theta_{e,cold}$ is a reference cold temperature and $\theta_{e,warm}$ is the warm engine temperature. Data for warm-engine emission rates $m_j^\circ$ are derived from engine tests and implemented in the same way as in the FOM. Other parameters are listed in Table 1.

TABLE 1

Engine and exhaust parameters

| Parameter | Value |
|---|---|
| $f_{\mathrm{CO}}$ | 2.2 |
| $f_{\mathrm{HC}}$ | 1.8 |
| $f_{\mathrm{NO}_x}$ | 0.8 |
| $\theta_{e,\infty}$ | 87 °C |
| $\theta_{e,warm}$ | 70 °C |
| $\theta_{e,cold}$ | -25 °C |
| $H_{\mathrm{CO}}$ | -10.1 MJ/kg |
| $H_{\mathrm{HC}}$ | 45.8 MJ/kg |
| $H_{\mathrm{NO}_x}$ | -12.5 MJ/kg |
| $AFR_{st}$ | 14.5 |

In the ROM, only the temperature level $\theta_e$ is considered, which lumps the thermal capacity of both the oil and coolant. This dynamic model reads:

$$C_e\dot{\theta}_e = P_{th,e}(\theta_e) - G_e \cdot (\theta_e - \theta_0) - P_{th,aux} \qquad (3)$$

where $C_e$ is an equivalent thermal capacity, $G_e$ an equivalent thermal conductivity, $\theta_0$ is the ambient temperature and $P_{th,e}$ is the sum of friction power dissipated into heat and thermal power transferred from the engine gas to the coolant

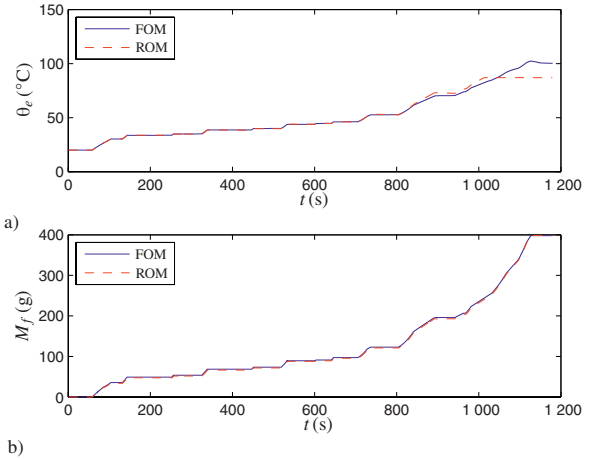


Figure 3

Calibration of the ROM against the FOM, a) engine temperature, b) cumulative fuel consumption.

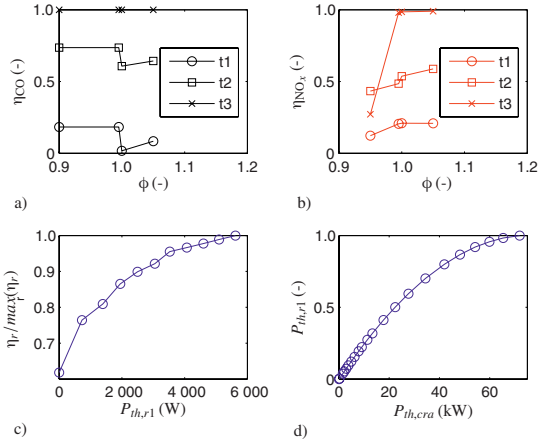


Figure 4

Tabulated data of the exhaust system, a) CO conversion efficiency (t1–t3: $\theta_c = \{216, 262, 773\}$ °C), b) $NO_x$ conversion efficiency (t1–t3: $\theta_c = \{205, 265, 405\}$ °C), c) Rankine cycle efficiency, d) power input to the Rankine system (normalized to its maximum value).

*(see Fig. 2b)* and $P_{th,aux}$ is the thermal power drained by the cabin heater. The dependence on speed and torque is not explicited. The external cooling system is not modeled, thus temperature $\theta_e$ is just supposed to be limited by the value $\theta_{e,\infty}$ at which an ideal thermostat is activated, $\theta_e \leq \theta_{e,\infty}$.

Numerical values for $C_e$ and $G_e$ have been fitted against the full-order model. Figure 3a shows the results of such fitting as a comparison between the FOM coolant temperature and the ROM $\theta_e$ with $G_e = 1$ W/K, $C_e = 54$ kJ/K. The corresponding cumulative fuel consumption $M_f$ is plotted in Figure 3b. These variations are calculated along the NEDC (New European Driving Cycle) with a cold start. The engine's speed and torque values calculated by the FOM, with the energy management strategy RB *(see Sect. 2.1)*, are fed into the ROM and its temperature, fuel consumption rate, etc. outputs are compared with the outputs of the FOM.

## 1.3 Catalyst Temperature

Emissions out of the catalyst are modeled in the ROM as:

$$m_j(u, \theta_e, \theta_c) = m_{j,e}(u, \theta_e) \cdot (1 - \eta_j(\theta_c, \phi)) \tag{4}$$

where $\phi = \phi(u)$ is the equivalence ratio of the engine combustion and $\eta_j(\cdot)$ is the conversion efficiency of $j$-th pollutant. These data are implemented as in the FOM, see Figure 2d for the equivalence ratio and Figure 4a, b for the conversion efficiency.

The equivalent catalyst temperature $\theta_c$ is described by the dynamic model:

$$C_c(\theta_c) \cdot \dot{\theta}_c = P_{th,ec} - P_{th,cr} - G_c \cdot (\theta_c - \theta_0) + P_{ch,c} \tag{5}$$

where:

$$P_{th,ec}(u, \theta_e) = m_{exh} \cdot c_{exh}(\theta_{exh}) \cdot \theta_{exh} \tag{6}$$

$$P_{th,cr}(u, \theta_e, \theta_c) = m_{exh} \cdot c_c(\theta_c) \cdot \theta_c \tag{7}$$

and $m_{exh} = m_f \cdot \left(\frac{AFR_{st}}{\phi} + 1\right)$. The exhaust temperature $\theta_{exh} = \theta_{exh}(u)$ is tabulated as a function of speed and torque as in the FOM, see Figure 2c. The heat released by the chemical reactions in the catalyst is $P_{ch,c} = \sum_j P_{ch,j}$, where $P_{ch,j} = -H_j \cdot \eta_j \cdot m_{j,e}$. All of the specific heat at constant pressure $c$ and the catalyst capacity $C_c = M_c \cdot c_c(\theta_c)$ are taken from the FOM where they are tabulated against respective temperature levels.

Numerical values for $M_c$ and $G_c$ have been fitted against the temperature of the catalytic wall predicted by the FOM. A comparison is shown in Figure 5a. Correspondingly, Figure 5b shows tailpipe CO emission rate as predicted by the FOM and the reduced-order model. As in the previous section, these results have been calculated over a NEDC, where the engine speed and torque values predicted by the FOM with strategy RB have been passed to the ROM as inputs. Additional model parameters are listed in Table 1.

## 1.4 Rankine-Cycle Heat Recovery

In both the full-order model and the reduced-order model, the Rankine-cycle power output is:

$$P_{el,r} = P_{th,r1} \cdot \eta_r(P_{th,r1}) \tag{8}$$

where $\eta_r(\cdot)$ is the Rankine system efficiency, see Figure 4c and $P_{th,r1}$ is the thermal power transferred from the exhaust

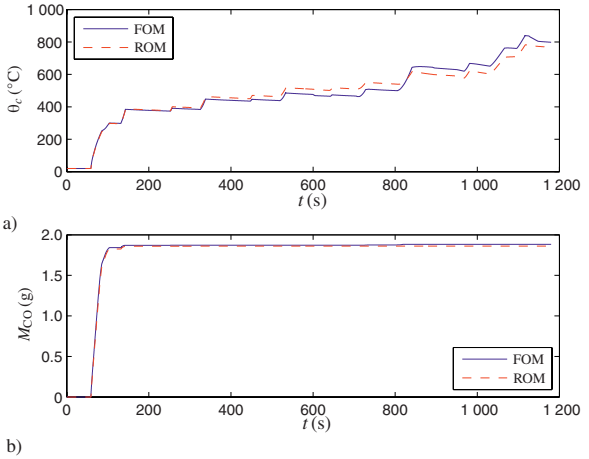


Figure 5

Calibration of the ROM against the FOM, a) catalyst temperature, b) cumulative CO emission.

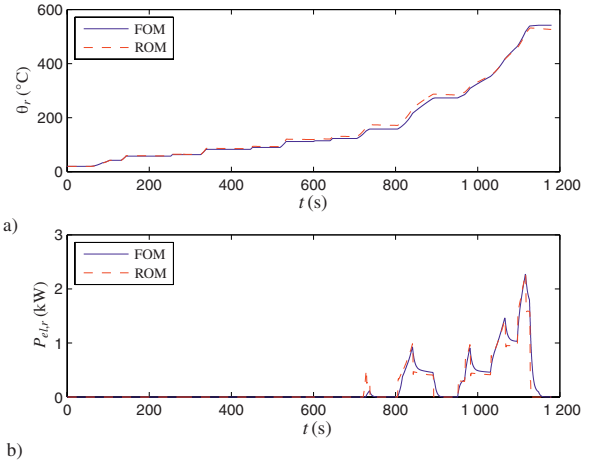


Figure 6

Calibration of the ROM against the FOM, a) Rankine-system pipe temperature, b) Rankine-system output power.

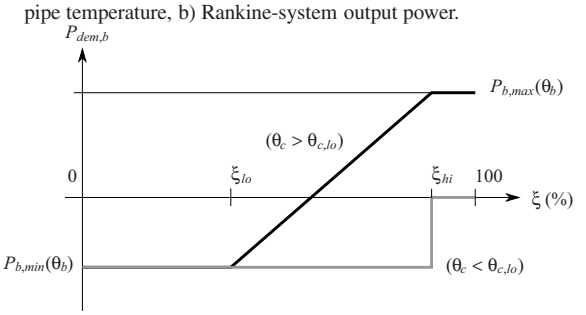


Figure 7

Schematic of the heuristic strategy RB: variation of $P_{dem,b}$ as a function of battery SOC.

pipe downstream of the catalyst to the Rankine cycle through the exchanger. The maximum value of $P_{th,r1}$ is a tabulated function of the available enthalpy in the exhaust gas, $P_{th,cra} = m_{exh} \cdot c_c(\theta_c) \cdot (\theta_c - \theta_{ref})$, where $\theta_{ref} = 100°C$, see Figure 4d. However, the Rankine system's activation depends on the exchanger temperature $\theta_r$. The system is only active when $\theta_r > 150°C$ and fully active, *i.e.*, the whole power (8) is produced, when $\theta_r > 170°C$.

The dynamics of $\theta_r$ read:

$$C_r\dot{\theta}_r = P_{th,cr} - P_{th,r2} - G_c \cdot (\theta_r - \theta_0) \qquad (9)$$

where $P_{th,r2} = m_{exh} \cdot c_{exh}(\theta_c) \cdot \theta_r$.

Numerical values for $C_r$ and $G_r$ have been fitted against the temperature trajectories calculated by the FOM. The comparison is shown in Figure 6a. Correspondingly, Figure 6b shows the Rankine-cycle output power as predicted by the FOM and the reduced-order model, using the same validation procedure as in the previous sections. The Rankine output power affects the electric power balance at the electric node. Neglecting the battery internal losses:

$$P_{el,b} = P_{el,m}(u,t) - P_{el,g}(u,t) + P_{el,aux}(t) - P_{el,r}(u,\theta_r) \quad (10)$$

## 2 ENERGY MANAGEMENT

### 2.1 Rule-Based Strategy (RB)

The heuristic stragey takes into account, in a sequential fashion, several managing rules dictated by vehicle-level and component-level specifications. For simplicity's sake, it can be roughly described by two threshold parameters, $P_{dem,b}$ and $P_{start,e}$ (losses in the electric chain are neglected in this description). The former parameter is a power contribution from the battery, which is subtracted from the driver's power demand $P_{me,v}$ as if it were to be delivered by the engine. Actually, the resulting $\tilde{P}_{me,v} \triangleq P_{me,v} - P_{dem,b}$ is compared with $P_{start,e}$; if $\tilde{P}_{me,v} < P_{start,e}$ and several other conditions are met, the engine will be turned off, otherwise it will be turned on. Both $P_{dem,b}$ and $P_{start,e}$ are parameterized as a function of SOC. Moreover, $P_{dem,b}$ is also a function of battery temperature and catalyst temperature. In particular, the battery is forced to accept recharge ($P_{dem,b} = P_{b,min}$), as long as the catalyst temperature is below the light-off value $\theta_{c,lo}$, so to enforce high engine loads and a fast rise of catalyst temperature. Figure 7 qualitatively depicts these variations.

### 2.2 Strategies Based on Pontryagin's Minimum Principle (PMP0–PMP3)

The optimal control strategies are based on Pontryagin's Minimum Principle. The problem is defined by a cost function that is to be minimized over a cycle and by the boundary

conditions. Four scenarios are considered in the following sections:
- warm engine, focus on consumption, no heat recovery (S0);
- cold start, focus on consumption, no heat recovery (S1);
- cold start, focus on emissions, no heat recovery (S2);
- cold start, focus on consumption, Rankine-based heat recovery (S3).

### 2.3 Baseline PMP (PMP0)

***Scenario S0***
The cost function to be minimized is:

$$J = \int_0^T m_f(\omega_e, T_e)\, dt \tag{11}$$

Since the system is a combined HEV, the control vector is $u = [T_e, \omega_e]$. The system dynamic is:

$$\dot{\xi} = \frac{I_b(u,t)}{Q_0} \tag{12}$$

with the global constaint $\xi(T) = \xi(0)$. A physical constraint links the power at the engine, motor, generator and final drive shafts, so that the battery power is a function of the control input and the power demand $P_{me,v}(t)$.

***Strategy PMP0***
Define the Hamiltonian function as:

$$\tilde{H}(u, \xi, s, t) = m_f(u) - \lambda(t)\dot{\xi}(u,t) \tag{13}$$

The Euler-Lagrange equation is then:

$$\frac{d\lambda}{dt} = -\frac{d\tilde{H}}{d\xi} = \lambda\frac{d\dot{\xi}}{\xi} \tag{14}$$

Under the approximation that $-\frac{d\dot{\xi}}{\xi} \approx 0$, $\lambda$ is constant. The Hamiltonian is rewritten as:

$$H(u, s, t) = P_{ch,f}(u) + s(t)P_{el,b}(u,t) \tag{15}$$

by setting $P_{el,b} = -\dot{\xi}Q_bU_{b,oc}$ and $s \triangleq \lambda H_f/(Q_bU_{b,oc})$, where $Q_b$ is the battery nominal capacity and $U_{b,oc}$ its open-circuit voltage.

### 2.4 PMP with Engine Thermal Dynamics (PMP1)

***Scenario S1***
The cost function is the same as (11), but now the fuel consumption rate $m_f = m_f(u, \theta_e)$.

***Strategy PMP1***
To optimally manage the system in cold-start cycles, the strategy PMP1 adjoins the dynamics of $\theta_e$ to the Hamiltonian:

$$\tilde{H}(\cdot) = m_f(u) - \lambda(t)\dot{\xi}(u,t) - \mu(t)\dot{\theta}_e(u, \theta_e, t) \tag{16}$$

To keep a formulation of the Hamiltonian in power units similar to that of (15), a new state variable is conveniently defined as $-C_e\theta_e$, so that its variation is described by the thermal power $P_{th,e} = -C_e\dot{\theta}_e$. Consequently, the Hamiltonian reads:

$$H(\cdot) = P_{ch,f}(u) + s(t)P_{el,b}(u,t) + p(t)P_{th,e}(u, \theta_e, t) \tag{17}$$

The Euler-Lagrange equation reads:

$$\frac{dp}{dt} = -\frac{dH}{d(-C_e\theta_e)} = \frac{dH}{C_e d\theta_e} = \frac{1}{C_e}\left(\frac{dP_{ch,f}}{d\theta_e} + p\frac{dP_{th,e}}{d\theta_e}\right) \tag{18}$$

The strategy PMP1 is equivalent to that presented in [22].

### 2.5 PMP with Engine and Exhaust Thermal Dynamics (PMP2)

***Scenario S2***
The cost function is now a weighted sum of fuel consumption and emission rate:

$$J = \int_0^T \left(1 - \sum_j \beta_j\right) m_f(u, \theta_e) + \sum_j \beta_j m_{j,c}(u, \theta_e, \theta_c) dt \tag{19}$$

where $j = \{\mathrm{CO}, \mathrm{HC}, \mathrm{NO}_x\}$. Since the temperature window for reduction in the catalyst is the same for all three pollutants, in the following, the set $\beta_1 = \beta$, $\beta_2 = \beta_3 = 0$ is used.

***Strategy PMP2***
Similarly to PMP1, the Hamiltonian is obtained as:

$$\begin{aligned} H(\cdot) = {} & (1-\beta)P_{ch,f}(u, \theta_e) + \beta P_{ch,\mathrm{CO}}(u, \theta_e, \theta_c) \\ & + s(t)P_{el,b}(u,t) + p(t)P_{th,e}(u, \theta_e, t) \\ & + q(t)P_{th,c}(u, \theta_e, \theta_c) \end{aligned} \tag{20}$$

where $P_{ch,j} \triangleq m_{j,c}H_f$. A new thermal power is defined as $P_{th,c} \triangleq -C_c\dot{\theta}_c$. Its dependence on $\theta_e$ is neglected. The Euler-Lagrange equations read:

$$\frac{dp}{dt} = \frac{1}{C_e}\left((1-\beta)\frac{dP_{ch,f}}{d\theta_e} + \beta\frac{dP_{ch,\mathrm{CO}}}{d\theta_e} + p\frac{dP_{th,e}}{d\theta_e}\right) \tag{21}$$

$$\frac{dq}{dt} = \frac{1}{C_e}\left(\beta\frac{dP_{ch,\mathrm{CO}}}{d\theta_c} + q\frac{dP_{th,c}}{d\theta_c}\right) \tag{22}$$

Note that the approach in [24] reduces to an approximation of PMP2 with $p \equiv 0$, $q \equiv 0$, while $\beta$ (actually representing $\beta_3$ in that paper) varies to achieve different compromises between fuel cost and ($NO_x$) emissions. On the other hand, the strategy used in [23] is equivalent to PMP2 with $\beta = 1$ and $p \equiv 0$, but $q(t) \neq 0$.

### 2.6 PMP with Engine, Exhaust and Heat Recovery Dynamics (PMP3)

***Scenario S3***

Cost function as in S1.

***Strategy PMP3***

The Hamiltonian reads:

$$H(\cdot) = P_{ch,f}(u) + s(t)P_{el,b}(u,t) + p(t)P_{th,e}(u,\theta_e,t) + r(t)P_{th,r}(u,\theta_r) \quad (23)$$

where $P_{th,r} \triangleq -C_r\dot{\theta}_r$. The Euler-Lagrange equations read:

$$\frac{dp}{dt} = \frac{1}{C_e}\left(\frac{dP_{ch,f}}{d\theta_e} + p\frac{dP_{th,e}}{d\theta_e}\right) \quad (24)$$

$$\frac{dr}{dt} = \frac{1}{C_r}\left(\frac{-dP_{el,r}}{d\theta_r} + r\frac{dP_{th,r}}{d\theta_r}\right) \quad (25)$$

## 3 SIMULATION RESULTS

In this section, results of HOT simulation runs for scenarios S0–S3 are presented and compared with strategy RB. Scenario definitions are listed in Table 2. In particular, fuel economy, emissions, SOC variations and temperature variations are analyzed. In order to compare different trajectories leading to different values of final SOC, fuel economy data are corrected to take into account overall SOC deviations with respect to the initial value. Corrected fuel economy is found by interpolation between actual runs with opposite SOC balance or using the equivalence factor $s$ to convert residual electrochemical energy into fuel.

TABLE 2

Definition of test scenarios S0–S3, with respect to a Cold Start (CS), the value of β, the presence of a Rankine System (RS). Y/N: Yes/no.

| Scenario | CS | β | RS |
|---|---|---|---|
| S0 | N | 1 | N |
| S1 | Y | 0 | N |
| S2a | Y | 1 | N |
| S2b | Y | 0.25 | N |
| S3 | Y | 1 | Y |

### 3.1 Hybrid Optimization Tool (HOT)

The optimal strategies are calculated with the software HOT (Hybrid Optimization Tool) developed at IFP Energies Nouvelles and presented, *e.g.*, in [26]. HOT uses a generic HEV structure that can be parameterized to represent various hybrid architectures, including the combined architecture of the system considered here. Until the 2011 version, only strategy PMP0 was applied. The optimal value of the equivalence factor $s$ is found using the bisection method. A new feature introduced in 2011 includes the possibility of setting strategies PMP1 to PMP3.

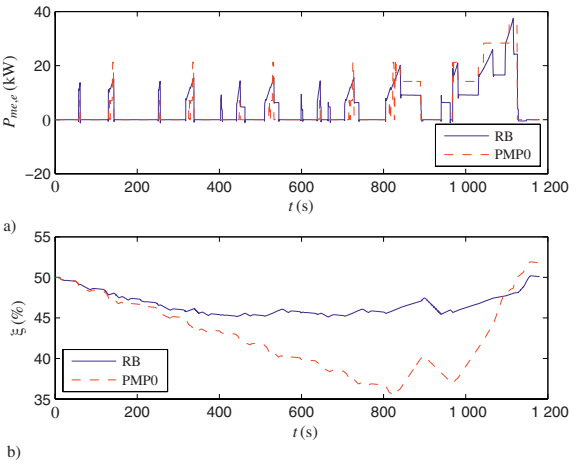


Figure 8

S0: comparison of strategies RB and PMP0 on the NEDC, a) engine output power, b) battery SOC.

### 3.2 Scenario S0

In this scenario, the strategies RB and PMP0 are compared. The latter is defined by the constant equivalence factor $s$. The optimal value found for the NEDC is $s = 2.925$.

Figure 8a shows the engine output power with the two strategies, while the corresponding SOC trajectories are plotted in Figure 8b. The strategy RB tends to use the engine more frequently and at lower loads. Consequently, the battery SOC varies less. In contrast, PMP0 leads to purely electric operation for a larger portion of the cycle. A charge-sustaining operation is obtained by operating the engine at high loads in the final, higher-efficiency section of the NEDC.

The fuel consumption with strategy RB is 4.52 L/100 km (SOC correction is negligible). With PMP0 it is 4.40 before SOC correction (Hybird Optimization Tool), and 4.26 after correction. The gain in fuel economy due to optimization is about 6%. One reason for this gain is the increased average engine efficiency, which is evaluated as 0.33 with RB, 0.34 with PMP0. Actually, the engine is operated at a few points with a relatively good efficiency with PMP0, while RB tends to follow a prescribed line in the speed-torque plane that maximizes the efficiency for every power output ("optimal operating line"). Since the choice of output power is driven by SOC considerations, RB operates the engine at points where the efficiency is low also. Such a behavior is clearly visible in Figure 9.

### 3.3 Scenario S1

In this scenario, the strategies RB, PMP0 and PMP1 are compared. The latter implies a constant $s$ and a variable $p(t)$.

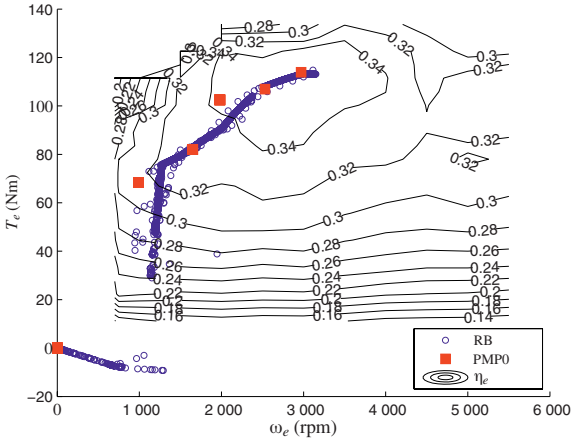


Figure 9

S0: comparison of strategies RB and PMP0 on the NEDC, engine operating points.

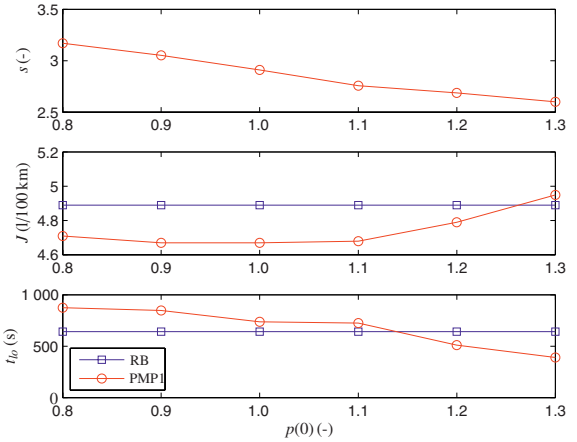


Figure 10

S1: comparison of strategies RB and PMP1 on the NEDC, a) optimal $s$, b) fuel consumption, c) catalyst light-off time, as a function of $p(0)$.

The two values $s$ and $p(0)$ are found using the following algorithm:

- set $p(0)$;
- set $s$;
- perform a cycle using PMP1;
- if $\xi(T) \neq \xi(0)$, adjust $s$ and return to 2;
- if $J$ is not min, adjust $p(0)$ and return to 1.

Figure 10a shows the dependence between $p(0)$ and the corresponding optimal $s$ for the NEDC. Such a dependence is explained by observing that increasing $p(0)$ makes the recharging of the thermal reservoir $\theta_e$ faster, thus the engine tends to be used more often. To counteract this trend, $s$ must decrease in order to favor the discharge of the battery. Such a basic behavior is predicted by the "toy" model of the Appendix and it is potentially relevant for online applications, as discussed further. For the NEDC, the values found by the algorithm above are $s = 2.91$ and $p(0) = 1$.

Strategy RB changes with respect to scenario S0 because it is sensitive to temperature. The priority now is to heat the catalyst. In contrast, the strategy PMP1 tends to "recharge" the thermal reservoir $\theta_e$ but less aggressively, since the cost function is given by the fuel consumption. This behavior is clearly visible in Figure 11a, b, showing the battery SOC and engine temperature trajectories obtained with the two strategies.

The fuel consumption with strategy RB is 4.82 L/100 km before SOC correction and 4.89 after correction. With PMP1 it is 4.53 before correction and 4.67 after correction. The reduction due to optimization is 4.5%. Interestingly, if strategy PMP0 is used in this scenario, the fuel consumption is 5.09 L/100 km, thus higher than when strategy RB is used.

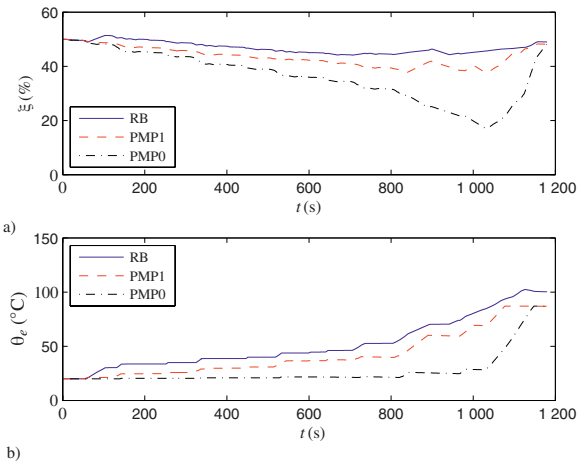


Figure 11

S1: comparison of strategies RB, PMP0 and PMP1 on the NEDC, a) battery SOC, b) engine temperature. Phases with SOC increase or temperature rise correspond to engine-on phases, while temperature or SOC decrease characterizes engine-off phases.

This fact confirms the interest of using a thermal-sensitive strategy for scenarios implying thermal transients.

Emissions are not included in the cost function in this scenario. However, the faster temperature rise obtained using PMP1 is also beneficial for emission reduction. Out-of-catalyst emissions are not modeled in S1, however the influence of the strategy can be forecasted by observing the

warm-up time $t_{wu}$, defined operatively as the time at which $\theta_e = 45°C$. Figure 10c shows that the $t_{wu}$ decreases for an increase of $p(0)$. Using the calibration $p(0) = 1$ that optimizes fuel consumption, the warm-up time is reduced with respect to PMP0 and thus the tailpipe emissions are likely to be reduced as well.

### 3.4 Scenario S2

In this scenario, strategy RB's behavior is the same as in scenario S1. The fuel consumption on the NEDC is 4.89 L/100 km and the CO emission is 1.88 g.

The behavior of strategy PMP2 is dependent on the choice of $\beta$. The case $\beta = 1$ (minimization of the emission) is considered first. As a basis of comparison, strategy PMP0 with an equivalence factor $s = 0.28$ would lead to a CO emission of 1.51 g. This result is obtained by concentrating the engine-on phase toward the last part of the cycle, rather than speeding up the rise of catalyst temperature, see Figure 12a, b. Using strategy PMP1 ($q(t) \equiv 0$), a result virtually identical to PMP0 is obtained, which is symptomatic of the engine temperature's relatively weak influence on the tailpipe emissions.

A slightly better result of 1.46 g is obtained using the strategy PMP2 and $p(t) \equiv 0$, for example by setting $q(0) = -0.1$ and $s = 50$. Now the strategy starts the engine at the very beginning of the cycle, when the vehicle is stopped, see Figure 12a, b. The power produced is partially charged into the battery, while the temperature of the catalyst rises rapidly. After this phase, the engine is kept off during the rest of the cycle. Using the complete PMP2 strategy, for example with $p(0) = 0$, $q(0) = 0$, the results are virtually identical.

For $\beta = 0.25$ (minimization of a weighted sum of fuel consumption and emissions), the cost function with strategy RB is 303 g. Despite its neglection of relevant dynamics, strategy PMP0 is already capable of attaining a similar result. With a choice $s = 2.965$ (and $p(t) = q(t) \equiv 0$), 1.67 g of CO and 4.87 L/100 km of fuel (corresponding to 402 g) are obtained, with a cost function of 302 g. Again, this result is obtained by limiting the engine-on phases and concentrating them toward the end of the cycle, rather than fastening the rise of catalyst temperature, since PMP0 is not temperature-sensitive *(see Fig. 13a, b)*.

With PMP1 ($q(t) \equiv 0$), a slightly better result is obtained with $p(0) = 0.8$, $s = 2.125$, namely, 2.15 g CO and 395 g of fuel (4.78 L/100 km) for a cost function of 296 g. With respect to the previous case with $\beta = 1$, fuel consumption is now included in the cost function and it is dependent on $\theta_e$, from whence the positive effect given by the introduction of such dynamics in the Hamiltonian. Indeed, the pattern of engine-on phases resembles that of PMP1 in scenario S1, Figure 11a. The rise of temperature is faster than with PMP0 but less aggressive than with RB. By switching to strategy PMP2, no further improvement has been found.

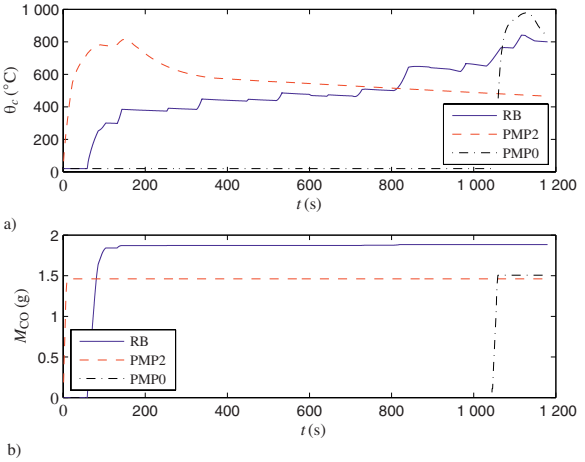


Figure 12

S2: comparison of strategies RB, PMP0, and PMP2 ($\beta = 1$) on the NEDC, a) catalyst temperature, b) cumulative CO emission. Phases with CO increase or temperature rise correspond to engine-on phases, while temperature decrease or zero CO emission characterize engine-off phases.

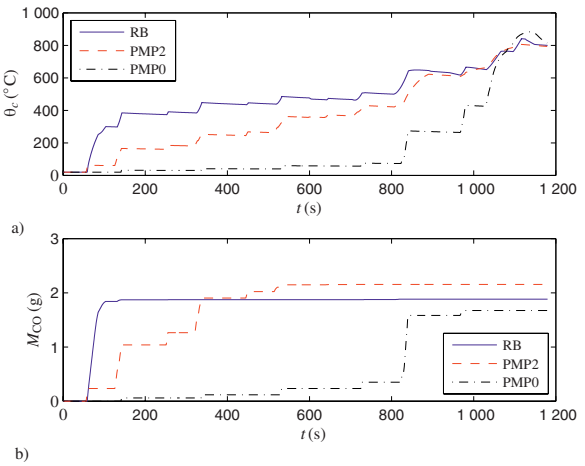


Figure 13

S2: comparison of strategies RB, PMP0 and PMP2 ($\beta = 0.25$) on the NEDC, a) catalyst temperature, b) cumulative CO emission. Phases with CO increase or temperature rise correspond to engine-on phases, while temperature decrease or zero CO emission characterize engine-off phases.

### 3.5 Scenario S3

For this scenario, strategy RB does not change. The overall results are only slightly different, with respect to the scenarios S1–S2, because now the SOC is affected by the recovered electric power. Fuel consumption is 4.71 after correction, while the amount of energy recuperated by the Rankine system is 220 kJ.

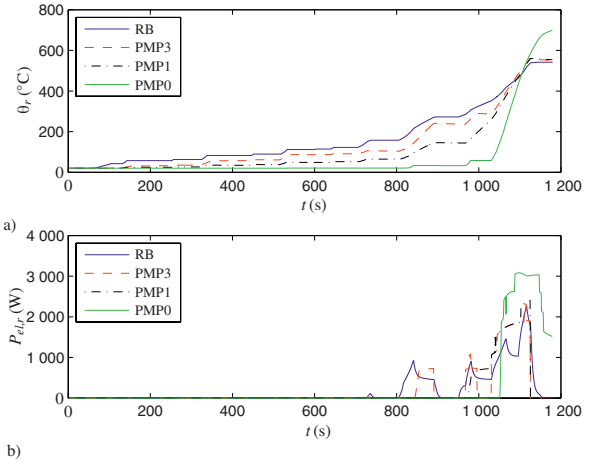


Figure 14

S3: comparison of strategies RB, PMP0, PMP1 and PMP2 on the NEDC, a) Rankine pipe temperature, b) Rankine electric power. Phases with CO increase or temperature rise correspond to engine-on phases, while temperature decrease or zero CO emission characterize engine-off phases.

With strategy PMP0, $p(t) = r(t) \equiv 0$, the fuel consumption is 4.89 L/100 km, thus higher than with RB. The rise of temperature in the exhaust pipe is actually too slow to allow enough electric power to be recovered. This behavior is clearly visible in Figure 14a, b. Since the recovered power is zero for pipe temperatures below 150°C, the first contribution to recovery occurs later with PMP0 than with RB.

In contrast, the use of strategy PMP1 ($p(0) = 1$, $r(t) \equiv 0$) leads to a reduction in fuel consumption that amounts to 4.50 L/100 km. However, introducing the exhaust pipe temperature dynamics and thus switching to PMP3 ($s = 2.91$, $p(0) = 1$ and $r(0) = 0$), only leads to minor improvements. Fuel consumption with PMP3 is actually 4.49 L/100 km after correction. Exhaust pipe temperature follows closer that obtained with strategy RB, the only difference being the early battery-charging phase commanded by RB but not by PMP3. Given that the energy recovered is slightly higher with the heuristic strategy (220 kJ with RB, 210 kJ with PMP3), the benefit in fuel economy is explained by a better average efficiency of the components using PMP3.

### 3.6 Overall

The results presented in the previous sections are summarized in Table 3. The table allows a comparison among the various strategies in terms of performed cost function, *i.e.*, fuel consumption for scenarios S0, S1, and S3 and the combined criterion for scenario S2. The benefits of using PMP1 instead of PMP0 appears clearly. On the other hand, the role of PMP and, to some extent, PMP3 is less clear and deserves further investigation.

TABLE 3

Performance criteria for the various scenarios considered

| Scenario | Units | RB | PMP0 | PMP1 | PMP2 | PMP3 |
|---|---|---|---|---|---|---|
| S0 | L/100 km | 4.52 | 4.26 | - | - | - |
| S1 | L/100 km | 4.89 | 5.09 | 4.67 | - | - |
| S2a | g | 1.88 | 1.51 | 1.51 | 1.46 | - |
| S2b | g | 303 | 302 | 296 | 296 | - |
| S3 | L/100 km | 4.71 | 4.89 | 4.5 | - | 4.49 |

## CONCLUSIONS AND PERSPECTIVES

The combination of powertrain energy management with powertrain–vehicle thermal management in HEVs is a topical control problem. Several heuristic strategies are being developed to approach this problem. Similarly to the contribution of optimal energy management to exploit the fuel economy potential of HEVs, optimal energy–thermal management could reveal highly beneficial to approach engine warm-up and cool-down, catalyst light-off, thermal accessories, heat accumulation, heat recovery.

In the paper, a general framework for optimal energy–thermal management has been presented. A system with a heat recovery system has been simulated under various scenarios, including cold start and heat recovery. Optimal strategies based on the Pontryagin Minimum Principle have been compared with a heuristic, rule-based strategy. The benefits in fuel economy and reduction of pollutant emissions that have been obtained are very promising. In a warmed-up cycle, PMP outperforms the heuristic strategy of 6% in fuel economy. For a cold-start cycle, the benefit of PMP is of 4.5%. In the presence of a Rankine-cycle heat recovery system, the benefit in fuel economy of is also about 5%. If emissions are considered, about 20% reduction is obtained with the PMP in a cold-start cycle. Finally, when a combination of fuel economy and emission reduction is considered as a criterion, the PMP-based strategy outperforms the heuristics as well.

The key factor of PMP strategies when cold-start conditions or a heat recovery system are considered is the addition of thermal dynamics to the instantaneous cost function, *i.e.*, the Hamiltonian function to be minimized. The offline estimation of the respective Lagrange multipliers or equivalence factors is very critical because, contrarily to the equivalence factor for battery energy, the equivalence factors for thermal energy vary during the cycle with an unstable dynamics.

In the paper, the optimal initial values of these equivalence factors has been found with a combination of shooting methods and direct search. Further work is necessary to derive a more general method that is capable of dealing with the problem complexities cited above. Further work is also needed to derive noncausal, *i.e.*, online applicable strategies. For the online applications, the equivalence factor of battery energy ($s$) could be adapted as in standard ECMS, while the equivalence factors for thermal energy would be related to $s$ through an offline-identified linear relationship as observed in Figure 10.

## REFERENCES


1 Sciarretta A., Guzzella L. (2007) Control of hybrid electric vehicles. Optimal energy-management strategies, *IEEE Control Syst. Mag.* **27**, 2, 60-70.

2 Marano V., Tulpule P., Stockar S., Onori S., Rizzoni G. (2009) Comparative Study of Different Control Strategies for Plug-In Hybrid Electric Vehicles, *SAE Paper* 2009-24-0071.

3 Guzzella L., Sciarretta A. (2011) Model-based Supervisory Control for Energy Optimization of Hybrid Electric Vehicles, *Control System Applications*, Vol. 2 of *The Control Handbook*, 2nd Edition, CRC Press, Boca Raton, FL.

4 Neuman M., Sandberg H., Wahlberg B., Folkesson A. (2009) Modeling and Control of Series HEVs Including Resistive Losses and Varying Engine Efficiency, *SAE Paper* 2009-01-1320.

5 Veneau N., Kefti-cherif A., Von Wissel D. (2002) Modeling and Control of Series HEVs Including Resistive Losses and Varying Engine Efficiency, *WIPO Patent Application* WO/2002/054159.

6 Dextreit C., Assadian F., Kolmanovsky I.V., Mahtani J., Burnham K. (2008) Hybrid Electric Vehicle Energy Management Using Game Theory, *SAE Paper* 2008-01-1317.

7 Back M., Terwen S., Krebs V. (2004) Predictive Powertrain Control for Hybrid Electric Vehicles, *SAE Paper* 2004-35-0112.

8 Willis F.G., Kaufman W.F., Kern G.A. (1975) Mechanical hybrid vehicle simulation, *SAE Paper* 790015.

9 Ao G.Q., Qiang J.X., Zhong H., Mao X.J., Yang L., Zhuo B. (2008) Fuel Economy and $NO_x$ Emission Potential Investigation and Trade-Off of a Hybrid Electric Vehicle Based on Dynamic Programming, *Proc. IMechE Part D: J. Automobile Engineering* **222**, 10, 1851-1864.

10 Lin C.C., Peng H., Grizzle J.W., Kang J.M. (2003) Power management strategy for a parallel hybrid electric truck, *IEEE Trans. Control Syst. Technol.* **11**, 6, 839-849.

11 Grondin O., Thibault L., Moulin Ph., Chasse A., Sciarretta A. (2011) Energy Management Strategy for Diesel Hybrid Electric Vehicle, *Proc. of the Vehicle Power and Propulsion Conference*, Chicago, IL, USA.

12 Serrao L., Onori S., Sciarretta A., Guezennec Y., Rizzoni G. (2011) Optimal Energy Management of Hybrid Electric Vehicles Including Battery Aging, *Proc. of the IEEE American Control Conference*, San Francisco, CA, USA.

13 Tulpule P., Stockar S., Marano V., Rizzoni G. (2009) Optimality assessment of Equivalent Consumption Minimization Strategy for PHEV Applications, *Proc. of Dynamic Systems and Control Conference*, Hollywood, CA, USA.

14 Vinot E., Trigui R., Jeanneret B. (2010) Optimal Management of Electric Vehicles with a Hybrid Storage System, *Proc. of the Vehicle Power and Propulsion Conference*, Lille, France.

15 Romaus C., Gathmann K., Böcker J. (2010) Optimal energy management for a hybrid energy storage system for EVs based on stochastic dynamic programming, *Proc. of the Vehicle Power and Propulsion Conference*, Lille, France.

16 Schacht E.J., Bezaire B., Cooley B., Bayar K., Kruckenberg J.W. (2011) Addressing Driveability in an Extended Range Electric Vehicle Running an Equivalent Consumption Minimization Strategy (ECMS), *SAE Paper* 2011-01-0911.

17 Opila D.F., Aswani D., McGee R., Cook J.A., Grizzle J.W. (2008) Incorporating drivability metrics into optimal energy management strategies for Hybrid Vehicles, *Proc. of the IEEE Conference on Decision and Control*, Cancun, Mexico.

18 Hellström E., Åslund J., Nielsen L. (2010) Management of Kinetic and Electric Energy in Heavy Trucks, *SAE Paper* 2010-01-1314.

19 Dib W., Serrao L., Sciarretta A. (2011) Optimal Control to Minimize Trip Time and Energy Consumption in Electric Vehicles, *Proc. of the Vehicle Power and Propulsion Conference*, Chicago, IL, USA.

20 Kolmanovsky I., Nieuwstadt M., Sun J. (1999) Optimization of complex powertrain systems for fuel economy and emissions, *Proc. of the IEEE Int. Conference on Control Applications*, Kohala Coast, HI, USA.

21 Tate E.D., Grizzle J.W., Peng H. (2010) SP-SDP for Fuel Consumption and Tailpipe Emissions Minimization in an EVT Hybrid, *IEEE Trans. Control Syst. Technol.* **18**, 3, 673-687.

22 Lescot J., Sciarretta A., Chamaillard Y., Charlet A. (2010) On the integration of optimal energy management and thermal management of hybrid electric vehicles, *Proc. of the Vehicle Power and Propulsion Conference*, Lille, France.

23 Chasse A., Corde G., Del Mastro A., Perez F. (2010) HyHIL: online optimal control of a parallel hybrid with after-treatment constraint integration, *Proc. of the Vehicle Power and Propulsion Conference*, Lille, France.

24 Kessels J.T.B.A., Willems F.P.T., Schoot W.J., van den Bosch P.P.J. (2010) Integrated Energy and Emission Management for Hybrid Electric Truck with SCR aftertreatment, *Proc. of the Vehicle Power and Propulsion Conference*, Lille, France.

25 Sciarretta A., Dabadie J.C., Albrecht A. (2008) Control-oriented Modeling of Power Split Devices in Combined Hybrid-Electric Vehicles, *SAE Paper* 2008-01-1313.

26 Chasse A., Sciarretta A. (2011) Supervisory control of hybrid powertrains: an experimental benchmark of offline optimization and online energy management, *Control Eng. Pract.*, accepted for publication.


*Final manuscript received in April 2012*
*Published online in September 2012*

## APPENDIX

The following "toy" model illustrates the main features of the optimisation scenario S1. Consider a system described by the following equations:

$$L(t) = \frac{1}{2}au(t)^2 - b\theta(t) \tag{26}$$

$$\dot{\xi}(t) = D(t) - u(t) \tag{27}$$

$$\dot{\theta}(t) = cu(t) - k\theta(t) \tag{28}$$

Consider an optimal control problem consisting of minimizing:

$$J = \int_0^T L(t)dt \tag{29}$$

with the global constraint:

$$\int_0^T \dot{\xi}(t)dt = 0 \tag{30}$$

Thus $L$ plays the role of $P_{ch,f}$, $\dot{\xi}$ of $P_{el,b}$, $u$ of $P_{me,e}$, $D$ of $P_{me,v}$, $\theta$ of $\theta_e$, while $T$ is the cycle duration. The model parameters $a$, $b$, $c$ and $k$ completely define the study.

### Solution

Build the Hamiltonian by adjoining the two dynamics with the multipliers $s$ and $p$,

$$H = \frac{1}{2}au(t)^2 - b\theta(t) + s(D(t) - u(t)) + p(cu(t) - k\theta(t)) \tag{31}$$

Euler-Lagrange equations:

$$\dot{s} = 0 \tag{32}$$

$$\dot{p} = -\frac{\partial H}{\partial \theta} = b + kp(t) \Longrightarrow \tag{33}$$

$$\Longrightarrow p(t) = -\frac{b}{k} + \left(p(0) + \frac{b}{k}\right)e^{kt} \tag{34}$$

Pontryagin Minimum Principle:

$$\frac{\partial H}{\partial u} = au(t) - s + cp(t) = 0 \Longrightarrow \tag{35}$$

$$\Longrightarrow u(t) = \frac{s - cp(t)}{a} = \frac{s}{a} + \frac{c}{a}\frac{b}{k} - \frac{c}{a}\left(p(0) + \frac{b}{k}\right)e^{kt} \tag{36}$$

Global constraint:

$$\int_0^T D(t)dt \triangleq E_d = \int_0^T u(t)dt \Longrightarrow \tag{37}$$

$$\Longrightarrow s = -\frac{bc}{k} + \frac{c}{kT}\left(p(0) + \frac{b}{k}\right)(e^{kT} - 1) + \frac{aE_d}{T} \tag{38}$$

from whence:

$$u(t) = M - Ne^{kt} \tag{39}$$

with:

$$M \triangleq \frac{c}{akT}\left(p(0) + \frac{b}{k}\right)(e^{kT} - 1) + \frac{E_d}{T} \tag{40}$$

$$N \triangleq \frac{c}{a}\left(p(0) + \frac{b}{k}\right) \tag{41}$$

and:

$$\dot{\theta} = cM - cNe^{kt} - k\theta \Longrightarrow \tag{42}$$

$$\Longrightarrow \theta(t) = \frac{cM}{k} - \frac{cN}{2k}e^{kt} + \left(\frac{cN}{2k} - \frac{cM}{k}\right)e^{-kt} \tag{43}$$

Now $J = f(p(0))$. Thus find the optimal $p(0)$ as:

$$\frac{dJ}{dp(0)} = 0 \Longrightarrow p(0) = -\frac{b}{k} + \frac{a}{c}N, \tag{44}$$

where:

$$N = \frac{\frac{bc}{k^2}(e^{kT} - 1) - \frac{bc}{k^2}(e^{kT} + e^{-kT} - 2)(\frac{1}{kT} + \frac{1}{2})}{\frac{a}{2k}(e^{2kT} - 1) - \frac{a}{k^2T}(e^{kT} - 1)^2} \tag{45}$$

After simple manipulations, one finds that $N = \frac{bc}{ake^{kT}}$ and thus $p(T) = 0$, as predicted by optimal control theory under the circumstance that the state variable $\theta$ is not constrained at time $T$. As a further consequence,

$$H(t) = -\frac{a}{2}M^2 + sD(t) + \frac{a}{2}N^2 - aNM \tag{46}$$

with:

$$M = \frac{E_d}{T} + \frac{N}{kT}(e^{kT} - 1) \tag{47}$$

The following properties of this toy model are also relevant for the real application:

- the dependence between $s$ and $p(0)$ is linear and increasing; increasing $p(0)$ would make the engine recharge the thermal reservoir faster; the charge sustaining requires an increase of $s$ to balance;
- the Hamiltonian solely depends on the disturbance $D(t)$; that circumstance could be used to evaluate $p(t)$ directly from the Hamiltonian, instead of integrating the Euler-Lagrange equation.